HST STIS OBSERVATIONS OF THE CENTRAL RADIO/X-RAY SOURCE IN THE COMPACT STARBURST GALAXY HENIZE 2-10

Eric Rohr[1], Mark Whittle[1] (advisor), Amy Reines[2] and Kelsey Johnson[1]
[1]Department of Astronomy, University of Virginia, Charlottesville, VA 22904
[2]Department of Physics, Montana State University, Bozeman, MT 59717

Abstract

Based on radio and X-ray observations, it has been suggested that a black hole of mass $\sim 5 \times 10^5\,M_\odot$ resides in the dwarf starburst galaxy Henize 2-10 (Reines et al., 2011; Reines & Deller, 2012; Reines et al., 2016). This unusual finding has important implications for the formation of massive black holes in the early universe since Henize 2-10 can be viewed as a low redshift analog to the first high-z galaxies. We present long-slit *HST STIS* spectra that include the central radio/X-ray source. While recent *VLT-MUSE* spectroscopic observations with $\sim 0\farcs7$ seeing show no change in ionization near the central source (Cresci et al., 2017), our higher spatial resolution *STIS* observations identify a distinct compact region at the location of the radio/X-ray source (RXS). Initial analysis reveals broader (FWHM $\sim$ 380 km s^{-1}) blue-shifted lines of low ionization. Our analysis focuses on two plausible scenarios: a low Eddington LINER-like AGN and a young (few decades) SNR.

1. Introduction

In today's universe, it seems that all *massive* galaxies, irrespective of Hubble type, harbor massive black holes (MBHs) at their centers (see Kormendy & Ho, 2013, for a recent review). Recently, MBHs have been identified in much lower mass galaxies (e.g., Reines et al., 2013), but whenever measurable these appear to have well-defined stellar nuclei (e.g. bulges, pseudobulges or nuclear star clusters), and are not, therefore, close analogs to the youngest galaxies in which the first seed black holes are though to have formed.

It was therefore of great interest when Reines et al. (2011) identified a candidate MBH in the blue compact dwarf galaxy Henize 2-10 (He 2-10; He2-10) and suggested the MBH causes the emission from both a non-thermal radio source identified by Johnson & Kobulnicky (2003) and a relatively luminous X-ray point source identified by Kobulnicky & Martin (2010). In fact, Kormendy & Ho (2013)'s review cited Henize 2-10 as the "poster child" for MBH discovery due to its position on the radio-X ray luminosity-luminosity plane, with an inferred black hole mass of $\sim 2\times10^6\,M_\odot$ using the "fundamental plane" relation from Merloni et al. (2003).

However, subsequent observations have complicated the simple interpretation of a massive black hole. For example, Very-Long Baseline Interferometer (*VLBI*) observations confirmed the RXS to be non-thermal and compact, with size $\lesssim 3\,\mathrm{pc}\times1\,\mathrm{pc}$, consistent with the base of a MBH-driven jet or a young supernova remnant (SNR; Reines & Deller, 2012). Although High Sensitivity Array (*HSA*) observations by Ulvestad et al. (2007) found no milliarcsecond sources in Henize 2-10, suggesting that if the RXS is an SNR then it must be $\gtrsim$ 10 yr in age. Furthermore, Reines et al. (2016) published new deep Chandra X-ray observations, and noted that the original X-ray source was in fact a nearby X-ray binary, and at the RXS location was a point source that was 200 times

weaker, undermining the strength of the original argument for an MBH, and raising the credibility of a young SNR. Recent Very Large Telescope (*VLT*) Multi Unit Spectroscopic Explorer (*MUSE*) observations by Cresci et al. (2017) of Henize 2-10 with 0.″7 seeing reveal no high-ionization lines at the RXS position which might have been expected for more luminous AGN such as Seyfert galaxies. They suggested that a young SNR better matches the more recent radio and X-ray observations.

Since the central region of Henize 2-10 is crowded and undergoing an intense starburst, higher spatial resolution spectroscopy is needed to reliably isolate the emission at the position of the RXS. With its superior spatial resolution, the Hubble Space Telescope (*HST*) provides an ideal opportunity to zero in on the emission from the central source, and help clarify its nature.

2. STIS: Observations, Reduction & Measurements

We use the *HST* Space Telescope Imaging Spectrograph (*STIS*) to obtain spectral images along two orthogonal slits (see Figure 1) using four gratings: G430L, G430M, G750L, G750M (north-south slit used G430M and G750M only). We use a half-integer dither to generate final spatial pixels of size $0.''025 \times 0.''2$, or 1 pc × 9 pc [spatial pixels]. We confirm the two slit locations by cross-matching the Hα emission in the spectral (*STIS*) and photometric Wide-Field Planetary Camera 2 (*WFPC2*) images. Prior astrometry already tied the central RXS to a weak Hα knot, which we confirm falls within both slits. Hence, we are confident our observations include the central RXS.

Along the slit, we fit reddened Starburst99 (Leitherer et al., 1999) synthesis models to the continuum and Balmer emission lines, deriving ages of $\sim 3-8$ Myr and dust absorption $A_V \sim 1-1.5$ mag, consistent with typical starburst regions. We measure the line strengths

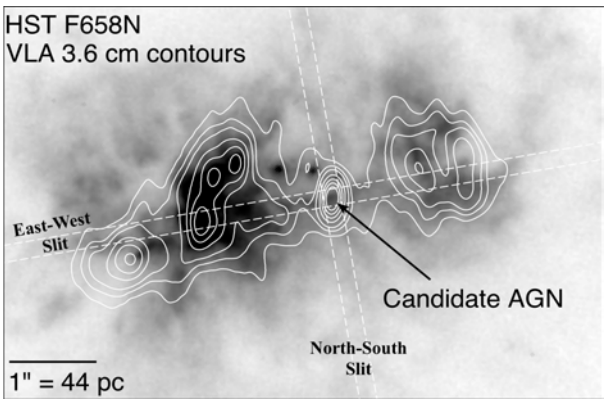

Figure 1: Gray: F658N filter Hα+continuum image from *WFPC2* on *HST*. White contours: *VLA* 3.6 cm radio (Reines et al., 2011). White dashed lines: two *STIS* slit locations.

from the RXS component after subtracting the Starburst99 starlight continuum and deblending the ambient H II emission using data from the adjacent pixels.

Figure 2 shows the continuum subtracted G750L spectral image for the EW slit. Although ambient H II emission from star formation is seen along the entire slit, *there is an additional component at the position of the RXS*. This emission clearly comes from gas with a significantly lower degree of ionization, with very strong [O I]λ6300 and [O II]$\lambda\lambda$7320, 30 lines. The G750M data (Figure 3) also reveals relatively broad, $\sim$ 380 km s^{-1}, blue wings at Hα, [N II]λ6548 and [O I]λ6300. Such blue asymmetric emission line profiles usually indicate expansion mixed with dust and are often found in both AGN and SNR spectra. We also note that despite identifying the RXS emission lines, we find no detectable high ionization lines such as [Ne V]λ3426 or [Fe V]λ5721. While this clearly rules out a more luminous Seyfert-like AGN, this is still consistent with emission from either a low-luminosity AGN (LLAGN) or an SNR.

3. STIS: Analysis and Results

Following standard practice, we use optical emission line diagrams to separate different

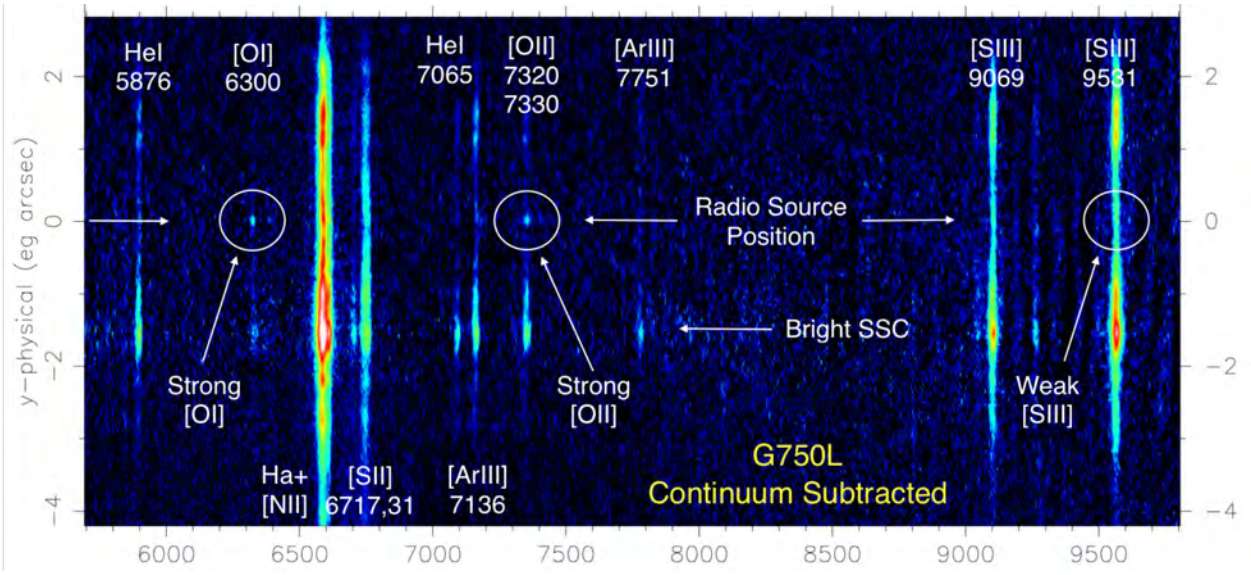

Figure 2: The continuum subtracted EW G750L *STIS* spectral image. The [O I]λ6300 and [O II]$\lambda\lambda$7319, 30 lines are strong at the RXS position. Conversely, the [S III]$\lambda\lambda$9069, 9531 lines are less enhanced. The slit also passes through a bright super-star cluster (SSC).

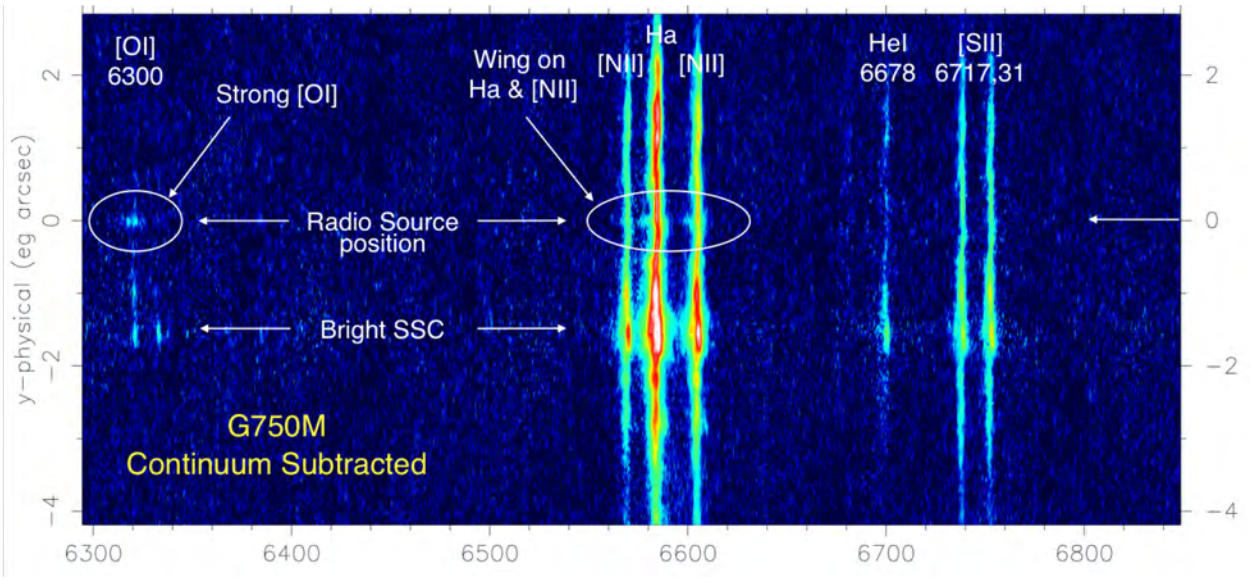

Figure 3: The continuum subtracted EW G750M *STIS* image. At the RXS position, blue wings are visible on the Hα and [N II]λ6584 lines, with profiles matching that of the strong [O I]λ6300 line.

classes of objects. Figure 4(a) shows the classical O-BPT diagram (Baldwin et al., 1981), clearly separating the RXS (red filled square) from the the surrounding star formation emission (open gold squares). It also confirms, along with the absence of other high excitation lines, that the RXS is not a Seyfert nucleus which would lie above and to the left. However, this diagram also reveals one of its major shortcomings: its inability to distinguish be-

tween several classes of object with strong low-ionization lines, namely young or old SNRs and low-luminosity AGN. For this reason, we have used the Supernova Catalog (Guillochon et al., 2016) to identify and measure line strengths for young SNRs, and hunted for line ratios that distinguish them from old SNRs and low-luminosity AGNs.

The Balmer (Hydrogen) line strengths of young SNRs depend strongly on the progenitor star. If the progenitor had a strong stellar wind, then for a few years the expanding supernova may not interact with any surrounding gas since it has been blown away. But once the shock reaches the neutral hydrogen gas the Balmer emission can greatly increase. Because of this, Balmer strengths in young SNRs vary greatly, so we seek line ratios without these lines. Based on the available data for the different objects and ability to separate different classes, we choose the line ratios shown in Figure 4(b). Unlike in Figure 4(a), the RXS falls with the young SNRs and away from the LINERs. We hope with more young SNR and LINER data that this diagram may ultimately resolve any ambiguity between these classes of objects.

While the RXS emission is marginally resolved spatially ($\sim 0\farcs1$), Figure 5 shows no detectable velocity gradient in either the east-west or north-south slits. If the gas is rotationally supported then a limit of ± 50 km s^{-1} across ± 1 pixel suggests that the mass of the black hole is $< 5 \times 10^5\,M_\odot$. If the RXS is a young SNR, then its linewidth FWHM ~ 380 km s^{-1} is quite low (typically a few $\times 10^3$ km s^{-1}) but within the observed range of Type IIn supernovae.

4. Multiwavelength Analysis

To help clarify whether the RXS more closely matches the properties of a young SNR or an LLAGN we need to fold in a range of other observations.

First, the deep Chandra X-ray observations by Reines et al. (2016) reduced the X-ray luminosity of the RXS by a factor of $\sim$ 200 of

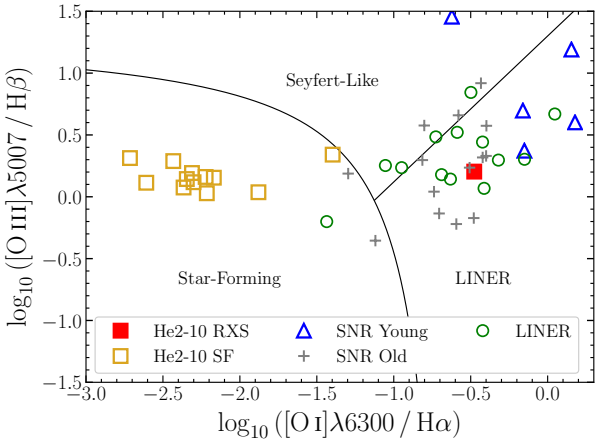

(a)

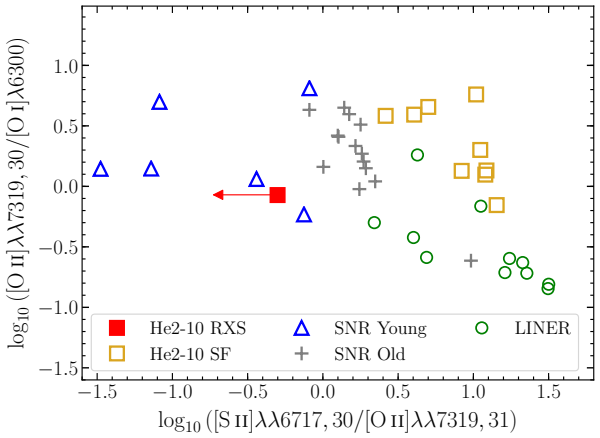

(b)

Figure 4: Line ratios were measured for Henize 2-10 from the STIS data; for young SNRs from data kindly provided by D. Milisavljevic and from the Open Supernova Catalog (Guillochon et al., 2016); and taken from the literature for old SNRs (Blair & Long, 2004) and LINERs (Ho et al., 1993). (a): Classical O-BPT diagram (Baldwin et al., 1981). Solid lines separating the three major object classes – Seyfert-like, Star-Forming and Low Ionization Nuclear Emission Region (LINER) – are taken from Kewley et al. (2006). (b): Our new low-ionization, non-Balmer emission line diagram that aims to separate the low ionization object classes. The young SNR located closest to the old SNR – at roughly (0.0, 0.8) – is Cas A, which is the oldest of the young SNR at ~ 350 yr.

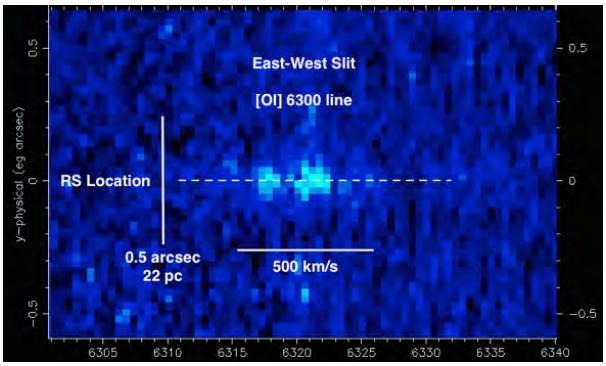

(a)

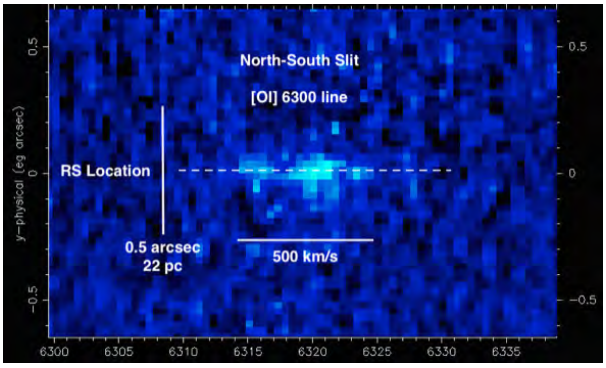

(b)

Figure 5: A zoom into the G750M spectral image of [O I]λ6300 at the location of the RXS for the east-west (a) and north-south (b) slits. While the emission is just resolved spatially, there is no indication of systematic rotation about either axis, placing a limit on orbital motion around a compact of object of $M < 5 \times 10^5\,\mathrm{M}_\odot$.

that originally reported by Kobulnicky & Martin (2010) – used by Reines et al. (2011) to conclude it as a MBH – by recognizing that the emission was dominated by a nearby, variable X-ray binary star. This shifted the location of the RXS on the X-ray-Radio luminosity-luminosity plot into a region that is consistent with young SNRs. However, this same location also lies just within the range occupied by AGNs with a flux ratio F_X/F_R that is close to the limit of the distribution found for AGN, including LLAGN. If the RXS is an LLAGN and it follows the AGN Fundamental Plane relation between L_X, L_R and M_BH (Merloni et al., 2003),

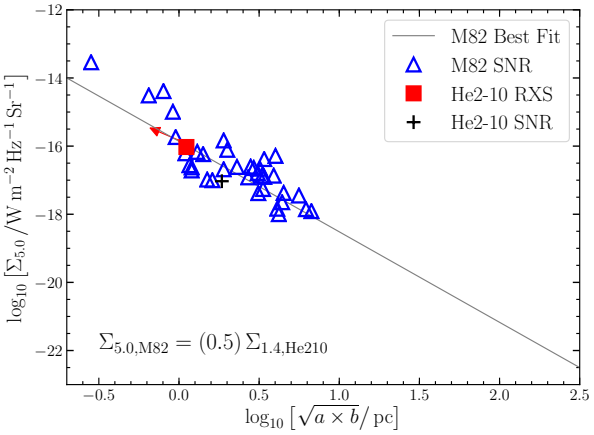

Figure 6: A comparison of the RXS and Henize 2-10's SNR to those of M82 (Fenech et al., 2008). We relate the observations of Henize 2-10 at a frequency 1.4 GHz to that of M82 at 5.0 GHz by assuming a constant power-law spectral index, hence the numerical factor of 0.5.

then the implied black hole mass is $\sim 10^8\,\mathrm{M}_\odot$. This is much larger than the original estimate (because the X-ray luminosity is much lower) and incompatible with the low measured gas and star velocity fields near the RXS. Nevertheless, there is considerable scatter in the $L_X - L_R$ plane and one cannot definitively rule out a low mass black hole LLAGN.

Second, one might ask whether the radio properties of the RXS match those of a young SNR or not. Using data on the radio fluxes and sizes of $\sim$ 36 young SNRs in M82, we find that the RXS in He 2-10 falls on the well-known relation between SNR surface brightness and size, the so-called $\Sigma - D$ relation (Figure 6; Fenech et al., 2008). We also took the radio flux distribution of the M82 SNRs and scaled their number of SNRs down to match the lower star formation rate in He 2-10, scaled their fluxes down to adjust to the greater distance of He 2-10 and then applied a cut at the the flux limit of the *LBA* radio observations of Reines & Deller (2012). Applying this cut, we estimate that Reines & Deller (2012) should have detected two young SNRs in He 2-10, which matches the two compact radio sources they did

in fact detect (one is the RXS; the other is located within a superstar cluster and is almost certainly a young SNR). Thus, the radio properties (luminosity and size) of the RXS match those expected for a young SNR. We still need to compile the radio properties of LLAGN to see of the RXS in He 2-10 might also match these properties.

Third, while SNRs have almost no optical or UV continuum, in the standard picture of AGN an accretion disk provides an X-ray to UV continuum that ionizes the surrounding gas to produce the emission lines. Thus, there should be a relation between either the X-ray or optical continuum and the flux in, for example, Hα. Using the STIS data, we estimate $< 5\%$ of the continuum light at the RXS location to be in a point source (compared to $\gtrsim 95\%$ from ambient star formation), and hence the equivalent width of the RXS Hα is > 480 Å. Adopting a power law (PL; $f_\nu \propto \nu^{-\alpha}$) for the ionizing spectral shape, and assuming full coverage of the source, we predict an Hα equivalent width in the range 120 and 720 Å for a PL index in the range 1.2 and 0.8 (typical for LLAGN; see Ho, 2008, for a recent review). Thus, this limit alone doesn't rule against an LLAGN. However, if we anchor the PL continuum to the new X-ray flux, then the predicted Hα flux is a factor $6 - 22$ below that observed. Adjusting the PL index to the measured $\alpha = 1.7$ now matches the observed Hα flux but would generate a visible UV and optical point source, which isn't seen. Thus, a simple power law LLAGN cannot simultaneously fit the observed continuum and emission line data. However, we still need to explore more realistic LLAGN continua shapes, which may include a UV bump that boosts the ionizing continuum without boosting the X-ray or optical.

5. Conclusions and Continuing Work

Our preliminary analysis shows that that the optical emission at the position of the RXS is clearly distinct from the ambient H II emission, which previous studies were unable to establish (Cresci et al., 2017). The cause of this emission is still unclear, though the preliminary analysis favors a young SNR over an LLAGN. However, there are still some tasks to be completed before any firm conclusion can be drawn.

First, we need to establish whether the RXS is at the geometric and kinematic center of the underlying older population galaxy, using existing *HST* and ground based imaging, and IFU and ALMA velocity maps. One expects LLAGN to reside at the center, but not a young SNR. Second, we will repeat our ionization analysis using a more realistic LLAGN spectral energy density (SED) rather than a simple power law. Third, we will map out the velocity and ionization structure along the *STIS* slit to look for any evidence of jet-driven outflows with associated shock ionization and/or triggered star formation. Finally, we will compile more X-ray and Radio data on young SNRs to see if the RXS in He 2-10 is more consistent with young SNRs or LLAGN.

Acknowledgements

Support for Program number HST-GO-12584 was provided by NASA through a grant from Space Telescope Science Institute, which is operated by the Association of Universities for Research in Astronomy, Incorporated, under NASA contract NAS5-26555. We thank R. A. Chevalier for valuable conversations regarding the nature of SNR. E.R. acknowledges support from the Virginia Space Grant Consortium, funded by NASA.

References

Baldwin, J. A., et al. 1981, PASP, 93, 5
Blair, W. P., et al. 2004, ApJS, 155, 101
Cresci, G., et al. 2017, A&A, 604, A101
Fenech, D. M., et al. 2008, MNRAS, 391, 1384
Guillochon, J., et al. 2016, ApJ, 835, 64
Ho, L. C. 2008, ARAA, 46, 475

Ho, L. C., et al. 1993, ApJ, 416, 63
Johnson, K. E., et al. 2003, ApJ, 597, 923
Kewley, L. J., et al. 2006, MNRAS, 372, 961
Kobulnicky, H. A., et al. 2010, ApJ, 718, 724
Kormendy, J., et al. 2013, ARAA, 51, 511
Leitherer, C., et al. 1999, ApJS, 1, 3
Merloni, A., et al. 2003, MNRAS, 1076, 1057
Reines, A. E., et al. 2012, ApJL, 750, 1
—. 2013, ApJ, 775, 116
—. 2016, ApJ, 830, L35
—. 2011, Nature, 470, 66
Ulvestad, J. S., et al. 2007, AJ, 133, 1868